Desalination and Water Treatment
www.deswater.com

doi: 10.1080/19443994.2015.1081627

57 (2016) 16703–16720
August

Taylor & Francis
Taylor & Francis Group

Amphistegina media filtration as pretreatment of SWRO desalination unit for producing different salinities to study the corrosion behavior of various materials

A.A. Bakr[a,*], K. Zakaria[a], M.A. Abbas[b], A. Hamdy[a]

[a]*Department of Analysis and Evaluation, Egyptian Petroleum Research Institute (EPRI), Nasr City, Cairo 11727, Egypt, Tel. +20 1227135228; emails: als_water@yahoo.com (A.A. Bakr), khaled209eg@yahoo.com (K. Zakaria) Tel. +20 1223517834; amalhamdy66@gmail.com (A. Hamdy)*
[b]*Department of Petroleum Applications, Egyptian Petroleum Research Institute (EPRI), Nasr City, Cairo 11727, Egypt, Tel. +20 1144764291; email: mohamedabbas1966@yahoo.com*

Received 1 December 2014; Accepted 4 August 2015

ABSTRACT

According to literatures, the corrosivity of many materials was studied in different aqueous environments (different salinities). In the present work, a semi-pilot seawater reverse osmosis (SWRO) desalination unit was assembled in EPRI and was used for producing seawater samples with different salinities (925, 4,845, and 18,975 mg/l TDS). The natural seawater sample was obtained from the Mediterranean Sea with salinity of 38,500 mg/l TDS and then, the samples with different salinities were obtained by mixing technique. *Amphistegina* tests (shells or hard parts) of the *Foraminifera* genus with mesh size 1.0–1.5 mm were separated directly by sieving from fresh beach sediments. *Amphistegina* media filtration system demonstrated good performance in removing particulates from the feedwater and producing permeate of acceptable quality for feeding reverse osmosis (RO) membrane at temperature 40˚C and flow rate 20 l/min. Operating the unit with addition of polyaluminum chloride coagulant at a concentration of 1.5 mg Al/l, enhances the performance of the RO unit. The produced filtrate has better SDI (<3), lower turbidity (less than 0.2 NTU), and higher TOC% reduction (97.1%, from 2.91 to less than 0.1 mg/l), while, the iron reduced from 1.82 to 0.05 mg/l. The susceptibility of Ni, Cu, and 70/30 Ni-Cu alloys for corrosion in the produced different seawater samples have been studied by weight loss measurements, potentiodynamic polarization, and electrochemical impedance spectroscopy methods. The surface analysis was carried out using scanning electron microscope and energy dispersive X-ray. The corrosion rate follows the order Cu > 70/30 Ni-Cu > Ni. Therefore, it was found that the desalination of seawater leads to enhancement of the water properties and decreases its corrosivity for all the studied materials.

Keywords: Desalination; Seawater; RO-membrane; *Amphistegina* tests; Filtration; Corrosion

*Corresponding author.

1. Introduction

Reverse osmosis (RO) systems are considered to be the most important improvement in desalination technologies and they are becoming increasingly popular due to their ease of operation, lower operational and maintenance costs, and environmental friendliness [1,2]. Compared with conventional surface and ground water treatment techniques, the RO desalination plants produce water with much lower concentrations of natural organic matter (NOM) and most of inorganic ions [3–6]. Therefore, the use of RO in desalination process has increased recently and RO process has become the leading technology in desalination market. The remarkable improvement of RO systems is mostly due to the incorporation of the energy recovery devices which significantly reduce the energy requirements and the improvements in the membrane material [7].

The conventional pretreatment in RO systems is not 100% secure to attend the recommendations of membrane manufacturers of feedwater quality. Bakr and Makled investigated the applicability of *Amphistegina* tests, which were collected from Marsa Matrouh coast on the southern coast of the Mediterranean Sea, instead of sand media filtration as a new pretreatment media for seawater desalination plants [8]. The *Amphistegina* test is coarsely perforate, lamellar, and flattened lenticular and it is often slightly contorted, biconvex, dorsoconvex, or ventroconvex. The peripheral outline is smooth or slightly lobulate. The main constituent of *Amphistegina* test is $CaCO_3$ with traces of $MgCO_3$, where the range of test size is 1.0–1.5 mm (n = 1,000 tests) and the main size is 1.2 mm [9].

The removal of iron from the groundwater and seawater prior to the membranes of desalination plants is the key step in the designing of these plants to avoid RO membrane fouling and scaling which are the most serious problems in the membrane processes [10]. However, the silt density index (SDI) is the main criterion of filtrate quality during the sequence of the pretreatment processes; Isaias [11] and Filmtec technical bulletin form of SW30HR LE-400 [12] found that the SDI of less than 5.0 was appropriate for the spiral-wound (SW) membranes. Different types of coagulants such as ferric chloride ($FeCl_3$) and ferric chlorosulfate ($FeClSO_4$) and polyaluminum chloride (PAC) were used. It was found that, the PAC has the minimal effect on the pH of seawater and is more efficient for removing particulates from raw seawater [8].

For many engineering materials, seawater is a very aggressive medium for the metals and it causes a severe corrosion damages to the metallic structures in very short time and the formed corrosion products could contaminate the surrounding environments (air, seawater, etc.). The most significant parameters that determine the corrosivity of seawater are the content of dissolved oxygen, water temperature, flow rate, salinity, pH, and the biological activity (bio-deposits) [13,14]. The importance of seawater as a mineral environment has increased during the last few decades because of offshore oil and gas explorations. Also, there is an increase in the applications of seawater desalination for fresh water production. Hence, the selection of construction materials for handling the seawater has been a problem [15]. The selection of materials for the various components of desalination plant is a major topic for continuing debate in the desalination community. Since the materials with higher durability are very expensive, the corrosion resistance is a crucial component of discussions on the impact of materials selection on capital and operational costs of distillation units [15].

Copper and its alloys have plenty of favorable properties such as electrical and thermal conductivity, mechanical workability, and corrosion resistance. These properties make them suitable for a wide range of applications in marine engineering [16,17]. Hence, they are used in a great variety of seawater systems such as production of shipbuilding, desalination plants, pipelines, condensers, and heat exchangers [18,19]. Nickel–copper alloys are characterized by good corrosion resistance, good weldability, and high strength; therefore, they have been used extensively as pipelines and structural materials. Also, they are widely used as corrosion-resistant materials in marine engineering [20,21].

In this study, the link between the corrosion and the produced desalinated water samples is investigated. The desalination unit consists of a recent technique called *Amphistegina* filter instead of a conventional sand filtration (used in the desalination plants). In a previous study, Hamdy et al. evaluated the corrosion behavior of the studied materials in natural seawater [22], while the major objectives of this study are to evaluate the replacement of the *Amphistegina* tests (as *Amphistegina* filter) instead of sand filter as a pretreatment media filtration for seawater desalination plants and to produce different seawater salinities by mixing technique. Thereafter, the effect of the produced seawater samples (different salinities) on the corrosion behavior of different materials was investigated.

2. Experimental

2.1. Semi-pilot seawater desalination unit

A semi-pilot unit was assembled and located at Egyptian Petroleum Research Institute (EPRI) and it

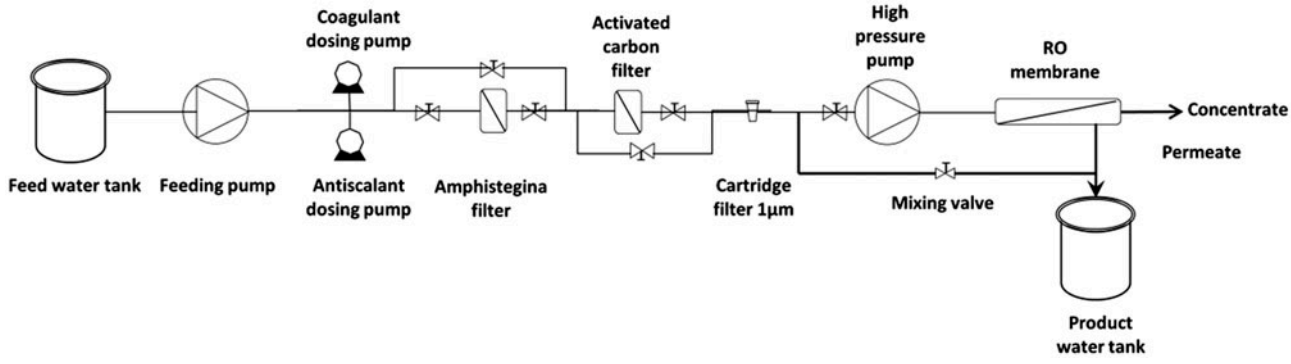

Fig. 1. Schematic diagram of the assembled semi-pilot seawater desalination unit.

was designed according to the schematic diagram shown in Fig. 1. The natural seawater was obtained from an open-intake in the Mediterranean Sea at Marsa Matrouh city then, it was fed to the unit. The desalination unit is capable of producing about 19.4 l/min and it consists of two feed and product water tanks (60 L). The RO systems operate on seawater and require an extensive pretreatment process in order to control the membrane fouling.

2.1.1. Flow rate and temperature

The high filtration rate leads to shorter filtration cycles and the filters may be plugged. The particles breakthrough was observed during filtration of feedwater from *Amphistegina* filter after 9.0 h of continuous operation. While, at higher operating temperature and with feeding the coagulant dosage, no solids breakthrough was observed under any operating condition. Therefore, at lower flow rate (20 l/min) and higher operating temperature (40˚C), the *Amphistegina* filter produces better filtrate [8].

2.1.2. Chemical pretreatment process

The chemical pretreatment is carried out using PAC as a coagulant and H_2SO_4 as antiscalant to maintain the pH value (chemical fed by dosing pump, 5 L-7 bar).

2.1.3. Granular media and cartridge filtrations

The feeding water pump (20–60 l/min) is followed by the dual media filter vessel (*Amphistegina* filter). This vessel is constructed of a fiberglass-reinforced polyester resin for standard water conditioning use with specific size (diameter 7.0 inches and height 17 inches), maximum operating pressure 150 psi (10.3 bars), maximum operating temperature 120˚F (49˚C), and the top opening of this vessel is 2½ inches. A dual media filter vessel was used and it has two layers of filtration media—typical design includes Anthracite [23] and *Amphistegina* [8]. The dual media filter vessel is followed by granular-activated carbon (GAC) filter [24]. Dual and carbon filters are manually controlled and followed by one 1 µm cartridge filter. The characteristics of *Amphistegina* filter media were reported such as particle size range (0.5–1.3 mm), effective size (0.8–1.2 mm), bed depth (22–32 inch), service flow rate (2–3.5 gpm/ft^2), backwash flow rate (10–18 gpm/ft^2), and backwash bed expansion (20–40%) [8].

2.1.4. RO membrane

Directly, one mixing valve takes the pre-treated water (filtrate) to the product water tank (permeate tank) crossing before the RO membrane for adjusting the required water salinity. The high pressure pump supplies the filtrate to the one membrane pressure vessel (housing) of the RO unit. The housing contains one Polyamide thin-film composite membrane (Filmtec SW30HR LE-400 seawater reverse osmosis membrane, SW type). The membrane nominal active surface area is 37 m^2, its permeate flow rate is 28 m^3/d (19.4 l/min), and the stabilized salt rejection is 99.75% [12]. The filter media used in the pretreatment of seawater are depicted in Fig. 2. The separation of feedwater into the low salinity product and high salinity concentrate is accomplished in the membrane unit.

2.1.5. Dilution operation

There are three flow meters in the unit to measure the filtrate of seawater (feed) and permeate of RO unit while the other flow meter is present for measuring the mixing of the filtrate volume to the final desalinated

Fig. 2. Pictures of the pretreatment media used in the assembled semi-pilot seawater desalination unit.

seawater product. Finally, the RO unit was controlled by an electrical control panel.

Dilution is the process of preparing a less concentrated solution from a more concentrated solution. The formal formula for calculating a dilution is $C_1V_1 = C_2V_2$, where C_1 and C_2 represent the concentrations of the initial and final solutions, respectively, and V_1 and V_2 represent their volumes [25]. From our study, C_1 is the concentration of the pretreated natural seawater (filtrate with 38,500 mg/l TDS), V_1 is the required volume of the filtrate, C_2 is the definite concentration of the final desalinated seawater concentration (925, 4,845, and 18,975 mg/l TDS), and V_2 is the volume of the final desalinated seawater concentration (60 L).

2.2. Corrosion procedures

The corrosion tests for Cu, Ni, and Ni-Cu materials in the seawater samples with different salinities, which produced from the desalination plant (which consists of the *Amphistegina* filter), will be discussed in the following subtitles.

2.2.1. Materials

Three different materials were selected in this study including Cu, Ni, and 70/30 Ni-Cu alloy. The composition of the specimens was analyzed by Portable X-ray Fluorescence (XRF) model NITON-XLt driven with software version 4.1. All the tested materials were provided by the Center of Metallurgical Research and Development Institute (CMRDI). The chemical analysis (in wt.%) of these materials are listed in Table 1.

2.2.2. Sample preparation

Rectangular test specimens of different materials, with 4 × 2 × 0.15 cm in dimension, were utilized in the experimental work for weight loss measurements. Prior to the experiment, all the specimens were abraded manually on successively finer silicon carbide emery papers with (350, 1,000, and 1,200) grit finish on all faces, degreased with acetone, rinsed in tap and distilled water, respectively, and finally dried in warm air.

Table 1
The chemical composition of the studied materials

Materials	Chemical composition, wt.% by elements					
	Ni	Cu	Mo	Fe	Cr	Mn
Cu	–	99.1	–	–	–	–
Ni	99.9	–	–	–	–	–
70/30 Ni-Cu	62.4	34.7	–	0.7	–	1.2

For potentiodynamic polarization measurements, each material was obtained in a rod form with 1.0 cm^2 exposed surface area as a working electrode. The samples were first embedded in epoxy resin and then polished successively with metallographic emery paper for increasing the fineness up to 1,200 grits. Then, they were washed with distilled water, decreased by ethanol and dried by cool air.

2.2.3. Corrosive media

The tested solutions are natural seawater obtained from the Mediterranean Sea (S_1) and the desalinated seawater samples produced by a semi-pilot desalination unit at EPRI (S_2, S_3, and S_4). The physicochemical properties of all seawater samples were determined according to the ASTM standard methods [26–30] and the results are given in Table 2. Cationic and anionic analyses were performed on the used seawater by ion chromatography, using DX 600 gradient IC system (Dionex, Sunnyvale, CA, USA). Integration was performed by Chromeleon Ver. 6.30 software (Dionex) and the results are listed in Table 3.

Table 2
Physicochemical properties of the natural and desalinated seawater samples

Properties	Seawater samples			
	S_1	S_2	S_3	S_4
pH @ 25°C	7.6	1.1	1.6	2.5
Conductivity, ohms/cm @ 23.7°C	5.6×10^{-2}	5.16×10^{-2}	1.674×10^{-2}	0.224×10^{-2}
TDS, mg/l	38,500	18,975	4,845	925
Hardness, mg/l	7,535	5,819	451	185
Salinity, mg/l	35,036	20,130	4,679	860
Turbidity, NTU	2.08	<0.2	<0.2	<0.2
TOC, mg/l	2.91	<0.1	<0.1	<0.1
$SDI_{15\ min}$[a]	6.4	<3.0	<3.0	<3.0

[a]15-min silt density index.

2.2.4. Weight loss measurements

The weight loss experiments were performed according to the standard method [31]. The losses in weight per area (ΔW, mg cm^{-2}) and the corrosion rates (C_R, mg cm^{-2}/d) over the exposure time were calculated from the following equations [32]:

$$\Delta W = (W_1 - W_2/A) \quad (1)$$

$$C_R = \Delta W/At \quad (2)$$

where ΔW is the weight loss of a material strip, A is the total area of a material strip, and t is immersion time (42 d).

2.2.5. Electrochemical techniques

Two electrochemical techniques, namely potentiodynamic polarization and electrochemical impedance spectroscopy (EIS) were used to study the corrosion behavior. The electrochemical measurements were carried out using Volta lab 40 potentiostat (Tacussel-Radiometer PGZ 301) and controlled by Tacussel corrosion analysis software model (Voltamaster 4) under static conditions. All experiments were conducted in a conventional three-electrode glass cells assembled with a platinum wire as auxiliary electrode, saturated calomel electrode (SCE) as reference electrode, and individual tested specimen as working electrode. All potentials given in this study were referred to the reference electrode.

Before the electrochemical measurements, each working electrode was immersed in the test solution for 30 min to establish the steady state, open circuit potential (E_{ocp}). After measuring the E_{ocp}, the electrochemical measurements were performed and the polarization curves were obtained in the potential range from −800 to −300 mV (SCE) at a scan rate of 2 mV/s.

EIS measurements were conducted in the frequency range between 100 kHz and 50 MHz using 10 steps per frequency decade at the corrosion potential after 30 min of immersion in the test solutions. Alternative current (AC) signal with 10 mV amplitude peak to peak was used to perturb the system. The data were analyzed using the Zsimpwin software program and EIS diagrams are given in the Nyquist representation. All experiments were performed in atmospheric condition without stirring at 303 K.

Table 3
Cationic and anionic analysis of the natural and desalinated seawater samples

Constituent, mg/l	Seawater samples			
	S_1	S_2	S_3	S_4
Chloride, Cl^-	21,234	12,200	2,836	521
Sodium, Na^+	11,583	5,701	1,677	218
Sulfate, SO_4^{2-}	3,009	871	141.8	6.48
Magnesium, Mg^{2+}	1,434	467	76	12
Calcium, Ca^{2+}	653	560	56	55
Potassium, K^+	388	155	53	13
Bicarbonate, HCO_3^-	145	0.41	–	–
Borate, BO_3	26	0.03	–	–
Total Fe	1.82	0.05	0.05	0.05

2.3. Surface analysis studies

The microscopic surface morphological examination and analysis of the elemental composition of the corrosion products were performed using SEM and EDX techniques, respectively.

2.3.1. Scanning electron microscopy

Surface morphology and roughness of the tested samples were examined by scanning electron microscope (SEM) after exposing to seawater for 42 d. The test was performed using JEOL model JSM-53000 scanning electron microscope (SEM).

2.3.2. Energy dispersive spectroscopy

The chemical composition of the surface film formed on the metal specimens was examined by energy dispersive X-ray (EDX). This was carried out with X-Max Oxford energy dispersive spectrometer conjugated with transmission electron microscope Jeol 2100. The spectra were recorded on samples immersed for a period of 42 d in all seawater samples.

3. Results and discussion

3.1. Efficiency of seawater desalination unit

3.1.1. Turbidity

In the conventional pretreatment process, the semi-pilot RO unit was equipped with an online PAC dosing pump. The experimental observations showed that PAC appeared to be the most promising coagulant to assist the performance of the media filtration and its dosing rate was 1.5 mg Al/l [8]. The data reported in Table 2 revealed that the much lower turbidity was less than 0.2 NTU resulted in case of *Amphistegina* filter and one 1-μm cartridge filter at 20 l/min and 40˚C as illustrated in Fig. 3. The turbidity was reduced from 2.08 NTU to 0.849 NTU in case of *Amphistegina* filter without coagulant, while it was reduced to 0.187 NTU in case of *Amphistegina* filter in presence of the coagulant.

3.1.2. Silt density index

SDI was used as main criterion of filtrate quality during the semi-pilot sequence of the pretreatment processes. SDI is widely used as an indicator in the desalination systems for measuring the fouling potential of seawater samples. While SDI of less than 5.0 was appropriate for the SW membranes [8,12], the mentioned configuration of the pretreatment system is effective in reducing the SDI of the natural seawater from 6.4 to a range of <3 SDI unit for the feedwater in the presence of PAC as shown in Table 2. From Fig. 3, at 20 l/min, 40˚C and in presence of 1.5 mg Al/l of PAC as coagulant, SDI values were reduced to 4.647 and 2.872 for *Amphistegina* filter without coagulant and *Amphistegina* filter in presence of the coagulant, respectively.

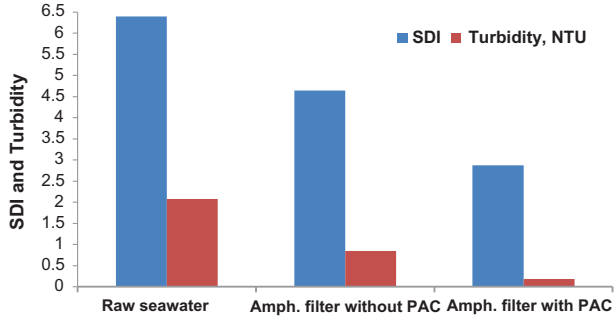

Fig. 3. Turbidity and SDI_{15} variations of *Amphistegina* filter with and without PAC (1.5 mg Al/l) at 20 l/min and 40˚C.

3.1.3. Typical performance of the used filters media

The adsorption of organic compounds from water is more common than the adsorption of inorganic compounds. By activated carbon, the adsorption of inorganic compounds from water is somewhat controversial and the adsorption of organic molecules from water is equally complicated [10,33,34]. The large macromolecules (turbidity and suspended solids) which present in the feedwater can be effectively accumulated by the coagulant and captured by the filtration media. In each vessel, the maximum bed capacity, which required to be filled, was 13.2 l. The dual-media filter vessel is followed by activated carbon filter with the same mechanical and operation specifications except for bed capacity required for each vessel (7.8 l and 6.6 l, respectively) and the two vessels are manually controlled. The characteristics of activated carbon filter media were reported such as particle size range (0.6–1.35 mm), effective size (0.55–0.75 mm), bed depth (66–76.2 cm), service flow rate (5.0 gpm/ft^2), backwash flow rate (10–12 gpm/ft^2), and backwash bed expansion (30–40%) [24]. GAC filter was followed by one 1 micron cartridge filter.

Fig. 4 represents the TOC measurements which were carried out in presence of 1.5 mg Al/l of PAC at high temperature and low flow rate. The total organic carbon in the natural sample (S_1) was 2.91 mg/l, as reported in Table 2, and the percentage of the total reduction of organic carbon by activated carbon filter was 73% (from 2.91 to 0.785 mg/l) and by activated carbon filter in the presence of PAC was 83.6% (from 2.91 to 0.476 mg/l). While, the best percentage of TOC reduction was 97.1% (from 2.91 to 0. 085 mg/l) by activated carbon and *Amphistegina* filters in the presence of PAC.

Also, from Table 3, the activated carbon filter was effective in the iron removal from seawater (1.82 mg/l). Fig. 4 indicates that all the studied media showed a definite removal of the iron even without

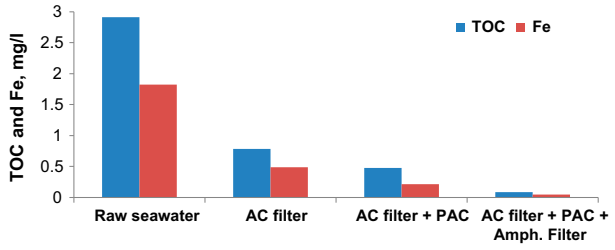

Fig. 4. TOC and iron removal by activated carbon (AC) filter with and without PAC (1.5 mg Al/l) and *Amphistegina* filter at 20 l/min and 40°C.

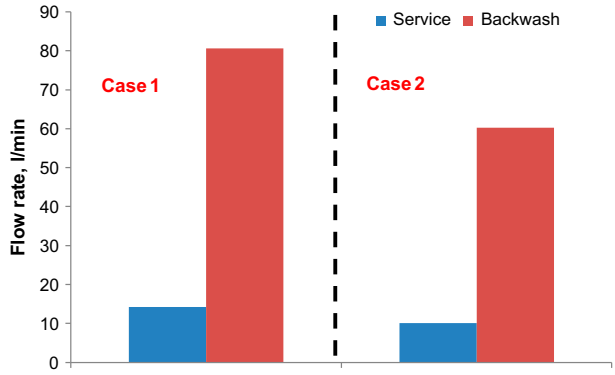

Fig. 5. Service and backwash flow rates of *Amphistegina* filter.

coagulant addition. The activated carbon filter removed a 0.486 mg/l without coagulant, but with addition of 1.5 mg Al/l of PAC at high temperature and low flow rate, the iron removal became 0.217 mg/l. While, the best iron removal was 0. 05 mg/l in case of activated carbon and *Amphistegina* filters with coagulant.

3.1.4. Service and backwash flow rates

The operation studies revealed that the filter became clogged by the retained particulates after the service period of filter (filter cycle), and it required cleaning. The filter cleaning took place by backwashing, using an upward high flow rate of seawater which is 10 times of service flow rate in case of conventional sand filter [8]. Therefore, the experimental data based on the performance of the *Amphistegina* bed during service and backwash flow rates are shown in Fig. 5. In case 1, when the service flow rate of *Amphistegina* filter was 14.2 l/min, the backwash flow rate required to clean the clogged *Amphistegina* bed was 80.6 l/min. While, in case 2, when the service flow rate of *Amphistegina* filter was 10.1 l/min, the backwash flow rate required to clean the clogged *Amphistegina* bed was 60.3 l/min. This figure represents that the backwash flow rate was only 5.7 times of the service flow rate of the *Amphistegina* filter with reduction of seawater consumption required to backwash process to 56.8%. Therefore, the bed expansion in the *Amphistegina* filter gave a better cleaning quality, extended the bed lifetime, and decreased a seawater consumption of backwash process.

3.1.5. The mixing technique

After the pretreatment process is complete, the different salinities of seawater samples were prepared by mixing technique. From Fig. 1, the dilution process takes place by a mixing valve which located before the RO desalination unit for mixing the filtrate to the final desalinated seawater product. By applying the calculating formula of dilution, the required volumes (V_1) of filtrate with 38,500 mg/l TDS (C_1) to mix a 60 L of the final desalinated seawater concentration (V_2) to produce a definite concentration (C_2) of the final desalinated seawater concentrations (925, 4,845 and 18,975 mg/l TDS) were calculated.

So, we need to use 1.44 L of the filtrate (S_1) to produce 60 L of 925 mg/l TDS (S_2). While, a 7.55 L is required to produce 60 L of 4,845 mg/l TDS (S_3) and a 29.57 L is required to producing a 60 L of 18,975 mg/l TDS (S_4).

3.2. Weight loss measurements

The variations of weight loss per unit area (ΔW, mg cm^{-2}) vs. time for Cu, Ni, and 70/30 Ni-Cu alloy coupons in the four tested media are shown in Fig. 6. A general trend is observed for the studied materials in all tested media, an increase in the values of ΔW with increasing time. The noticed high values of weight loss in natural seawater compared to the desalinated samples are due to the aggressive attack of the chloride ions to the material's surface.

Table 4 shows the calculated corrosion rates of the tested materials in the different media with variable salinities. It is clearly shown that copper has the maximum corrosion rate in all tested media, while the nickel exhibits lowest corrosion rate. In general, all the test materials show lower corrosion rates in the desalinated seawater samples compared to those obtained for the same materials in natural seawater. Generally, there is an understandable tendency in relation to localized corrosion to assume that the decreases in seawater salinity represent that there is a less aggressive environment. The data reported in Table 4 show that the effectiveness of the salinity on the corrosion behavior of the tested materials follows the order Cu > Ni-Cu > Ni.

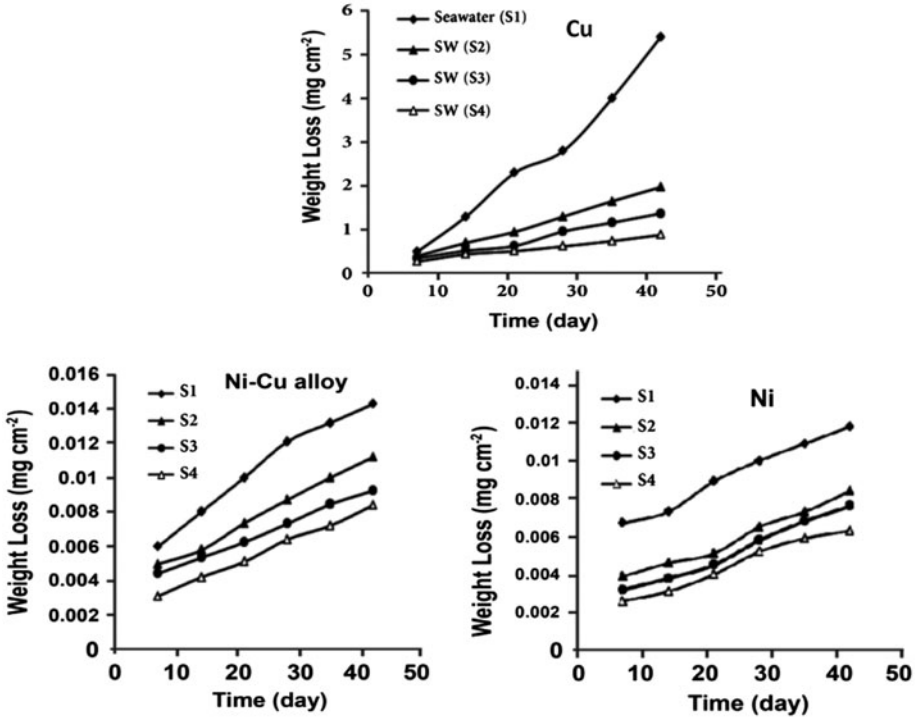

Fig. 6. Weight loss as a function of time for the tested materials after immersion in different media.

Table 4
Corrosion rates obtained from weight loss measurements for Cu, Ni, and 70/30 Ni-Cu in different seawater samples at a maximum immersion time (42 d)

Material	Corrosion rate (mg cm^{-2}/d)			
	Natural seawater (S_1)	S_2	S_3	S_4
Cu	0.12800	0.04700	0.0330	0.02100
Ni-Cu	0.00034	0.00026	0.00022	0.00020
Ni	0.00028	0.00020	0.00018	0.00015

It was proposed that in natural seawater, the initial corrosion product of copper is cuprous chloride, which reacts to produce a porous layer of cuprous oxide, Cu_2O (Cuprite) which was the main constituent of thick scales [35]. The cuprous oxide was generally oxidized over time to cupric hydroxide ($Cu(OH)_2$), atacamite ($Cu_2(OH)_3Cl$), or malachite ($Cu_2(OH)_2CO_3$). Owing to the buffering properties of seawater resulted from the presence of carbonate/bicarbonate and borate ions, the formation rate of cuprous oxide in seawater solution is lower and the generation rate of cuprous complexes (and thus the general dissolution rate) is higher than in the desalinated solutions, indicating the appearance of corrosion products $Cu_2(OH)_3Cl$ and $Cu_2(OH)_2CO_3$, which is in accordance with the EDX results.

These formed corrosion products cannot provide a good protection to the substrate because of their loose microstructure and they are not compact enough to decrease the chloride ion attacks [36], which accounts for the maximum value of the copper corrosion rate in natural seawater sample. Moreover, the increase of immersion time indicates the occurrence of pitting corrosion due to further formation of atacamite and the pits could be seen with the naked eye after corrosion products were removed from the copper surface.

The noticed increase in Ni and 70/30 Ni-Cu alloy resistances in seawater is attributed to the formation of a passive film and/or corrosion products, which gets thicker with time and could lead to the decrease in the corrosion rate. The passivation of nickel and 70/30 Ni-Cu alloy may be due to oxide film formation

which involved a dissolution–precipitation process at the active passive transition of nickel. Also, it was noticed that the corrosion behavior of nickel and the nickel-base alloy was less affected by the decrease in salinity than copper. This may be attributed to the stability of the protective layer formed on nickel and the nickel-base alloy in all the tested media [37,38].

3.3. Potentiodynamic polarization measurements

In order to understand the mechanism of the observed corrosion behavior, the potentiodynamic polarization curves for various studied materials, Cu, Ni, and 70/30 Ni-Cu alloy, in natural seawater sample and for comparison in desalinated seawater samples were evaluated and given in Figs. 7(a–d) and 8(a–c). The anodic and cathodic current–potential curves are extrapolated up to their intersection at a point where the corrosion current density (i_{corr}) and corrosion potential (E_{corr}) are obtained [39]. The corrosion potential (E_{corr}) is the voltage difference between a metal immersed in a given environment and an appropriate standard reference electrode. At the corrosion potential, the rate of hydrogen evolution is equal to the rate of metal dissolution, and this point corresponds to the corrosion rate of the system expressed in terms of current density [40]. Electrochemically, corrosion rate measurement is based on the determination of the oxidation current at the corrosion potential. This oxidation current is now called the corrosion current. (i_{corr}).

Also, the slopes of the anodic and the cathodic Tafel lines of the polarization curve were obtained (β_a and β_c, respectively). Another corrosion parameter is the polarization resistance (R_p), which is the transition resistance between the electrodes and the electrolyte; it can be defined as the slope of the linear part of the polarization curve close to the corrosion potential (E_{corr}). The corresponding corrosion parameters are listed in Table 5.

3.3.1. Influence of metal/alloy type

Fig. 7(a) shows a set of potential, E, vs. logarithm plots of the absolute value of the current density, I_{corr}, for Cu, Ni, and 70/30 Ni-Cu in natural seawater sample. Cu displayed a rapid current density increase with potential in the anodic branch, indicating the presence of a less protective oxide film in natural seawater. On the contrary, Ni and Ni-Cu followed a nonlinear trend at high anodic overpotentials, due to the formation of a passive surface. Differently to Ni and 70/30 Ni-Cu, the Cu metal denoted a sudden increase of the current density, attributed to the formation of a less protective oxide layer and a tendency to break down the oxide film and to develop pitting corrosion [41]. The cathodic branches for Ni and 70/30 Ni-Cu displayed a linear trend at high cathodic overpotentials. It is worth noting that the natural seawater is a rather complex mixture of many constituents and some of them may also contribute to the corrosion of the investigated metals even at low concentrations, for example, chloride ions or even the presence of sulfate ions [42].

Table 5 summarizes kinetic data calculated from Tafel plots. The most important feature is the difference in corrosion current densities (I_{corr}) in natural seawater sample for Cu, Ni, and 70/30 Ni-Cu alloys, that were 33.6, 4.3, and 18.0 $\mu A/cm^{-2}$, respectively. It is clearly noticed that the Cu has the maximum corrosion current density and hence the corrosion rate in all four seawater samples while the Ni exhibited the lowest corrosion rate. These results are in agreement with the data obtained from weight loss measurements. Moreover, the results showed that the 70/30 Ni-Cu alloy corroded at a higher rate than Ni in natural seawater, due to the presence of Cu as an alloy element.

The same trend was obtained in the desalinated seawater samples as shown in Fig. 7(b–d); this corrosion behavior appears to depend mainly on chemical composition of the exposed tested material. The decrease in the corrosion rate for Ni-Cu alloy more than Cu can be attributed to the incorporation of Ni ions in the mobile vacancies of the Cu_2O film decreasing the possibility of Cu dissolution from the alloy surface. Interestingly, Ni has a better corrosion resistance than Cu and Ni-Cu alloy in the seawater environments and the observed order of corrosion rate was Cu > 70/30 Ni-Cu > Ni.

3.3.2. Effect of seawater salinity

The data listed in Table 5 indicate that with decreasing the salinity value, the corrosion potential moved toward slightly positive values, the corrosion currents decreased and therefore the corrosion rates became slower. When these materials were immersed in different seawater salinities, the passivating phenomena can be observed in polarization curves as shown in Fig. 8(a–c). The passive phenomenon became weaker in the natural seawater sample.

As expected, the corrosion current densities for all studied metals and alloy were found to be much higher in the natural seawater than those in the desalinated waters especially in the case of Cu. This was presumably due to the fact that the natural seawater

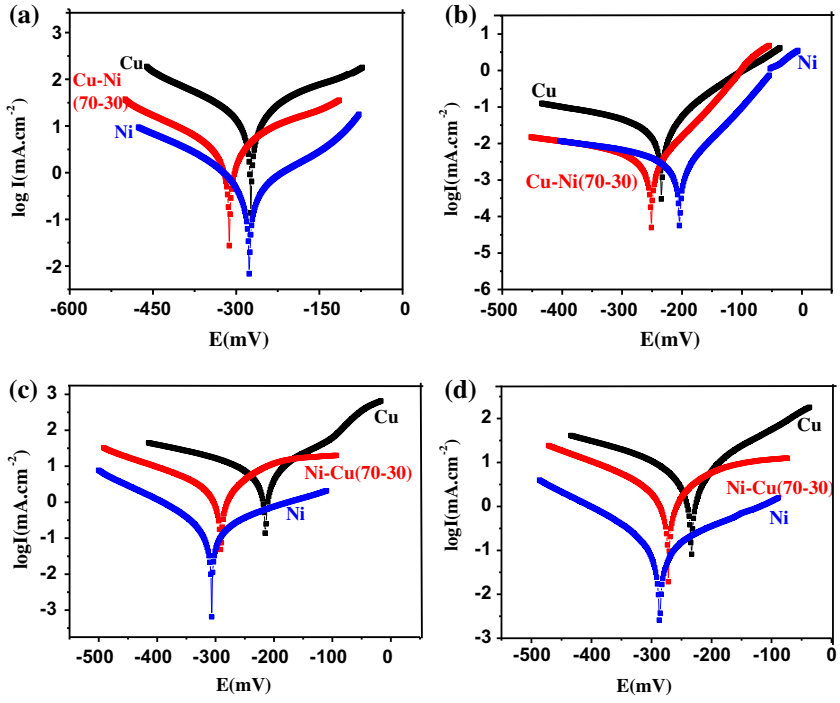

Fig. 7. Potentiodynamic polarization curves of the studied materials in different sea water solutions: (a) natural seawater S_1, (b) S_2, (c) S_3, and (d) S_4.

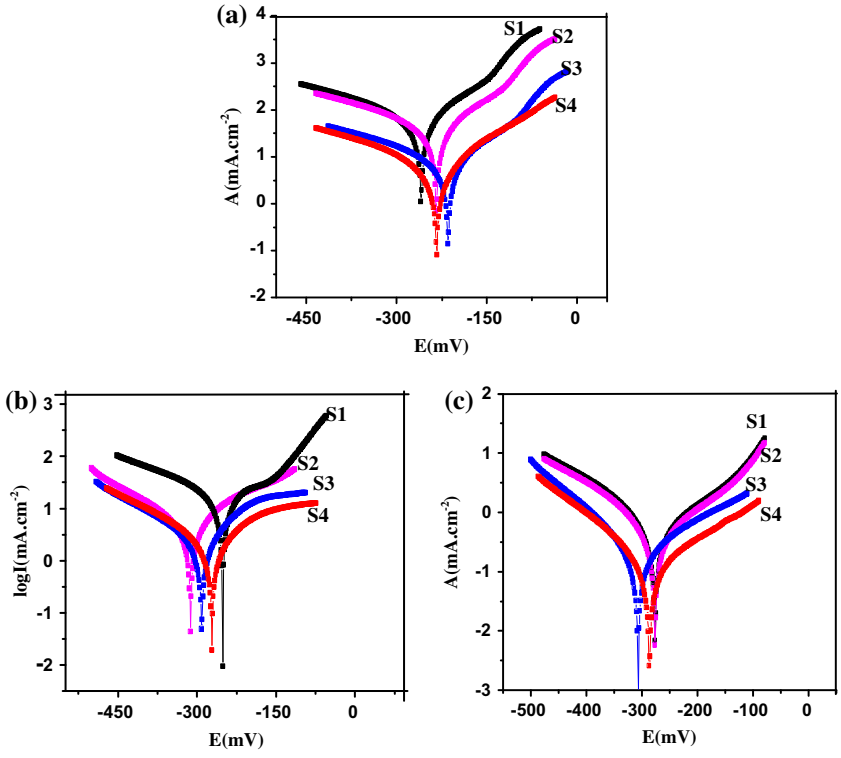

Fig. 8. Potentiodynamic polarization curves of the studied materials in different seawater solutions: (a) Cu, (b) 70/30Ni-Cu, and (c) Ni.

Table 5
Electrochemical parameters derived from polarization curves for the studied materials in different seawater environments

Parameters	S_1			S_2			S_3			S_4		
	Cu	70/30 Ni-Cu	Ni	Cu	70/30 Ni-Cu	Ni	Cu	70/30 Ni-Cu	Ni	Cu	70/30 Ni-Cu	Ni
E, mV	−259	−312	−276	−234	−251	−204	−215	−291	−307	−234	−271	−286
I_{corr}, mA/cm^{-2}, $\times 10^{-4}$	336	180	43	211	120	8	90	75	2.4	78	48	1.6
β_a, mV/decade	91	133	66	99	190	219	104	975	212	145	887	213
β_c, mV/decade	352	272	456	273	186	196	286	468	132	281	401	145
R_p, ohm/cm^{-2}	1,030	1,870	8,610	1,800	5,970	55,120	4,050	11,660	138,200	6,420	14,180	213,400

sample has higher salinity than desalinated one. The main effect of seawater salinity on the corrosion behavior results from its influence on the conductivity of water and also, from the influence of chloride ions on the breakdown of the passive films. With increasing the salinity, more readily chloride ions can succeed in penetrating the passive film and hence initiate pitting and crevice corrosion at localized sites on the metal surface, where oxygen adsorbed on the metal surface is displaced by chloride ions [43,44]. The small diameter of Cl^- enables penetration through the protective oxide film and the exchange of oxygen by chloride ions occurred at the sites where the metal-oxygen bond is the weakest. The accelerating effect of Cl^- ions may be due to the introduction of Cl^- ions from the solution into the oxide film, which formed in seawater sample, degrading its protective nature leading to pitting corrosion which can be explained by a competitive adsorption mechanism, in which chloride ions move into the double layer of the electrode surface to displace adsorbed oxygen species. The adsorbed Cl^- increases the potential difference across the passive film, thereby enhancing the metal ion diffusion from the metal/film interface to the film/solution interface forming cation vacancies at the metal/film interface [45–47].

The voids will be developed at the metal/film interface when Cl^- concentration is large and the continued growth of a void results in localized collapse of the passive film, which will dissolve faster than other regions of the passive film, leading to pit growth ultimately substrate alloy dissolution. Thus, the increase in corrosion rate with the increasing chloride ion concentration was attributed to the participation of chloride ions in the dissolution reaction [48]. However, Ni and 70/30 Ni-Cu alloy have very low corrosion rates that were not significantly affected by the decrease of salinity.

3.4. Electrochemical impedance spectroscopy

The EIS is conducted to confirm the trends of the corrosion rates determined by potentiodynamic polarization method [49]. The data obtained from the EIS measurements were plotted in the form of Nyquist plots, i.e. imaginary and custom real impedance. The impedance data were analyzed using software provided with the impedance system where the dispersion formula was used. For a simple equivalent circuit model consisting of a parallel combination of a capacitor, C_{dl}, and a resistor, R_{ct}, in series with a resistor, R_s, representing the solution resistance and the electrode impedance, Z, is represented by the mathematical formulation:

$$Z = (R_s + R_{ct}/1) + (2\pi f R_{ct} C_{dl})^n \quad (3)$$

where n denotes an empirical parameter $(0 > n > 1)$ and f is the frequency in Hz. The dispersion formula takes into account the deviation from the ideal capacitor, RC, behavior in terms of a distribution of time constants due to surface inhomogeneities, roughness effects, and variations in the properties or compositions of surface layers [50,51]. The impedance data were analyzed using the equivalent circuit model presented in Fig. 9. Various parameters such as solution resistance (R_s), the charge transfer resistance (R_{ct}), double-layer capacitance (C_{dl}) were calculated for the investigated materials in different seawater samples, and the data are presented in Table 6**.** The charge-transfer resistance (R_{ct}) values were calculated from the difference in impedance at low and high frequencies [39], while the values of double layer capacitance (C_{dl}) were obtained at the frequency f_{max}, at which the imaginary component of the impedance is maximal using the following relationship [52]:

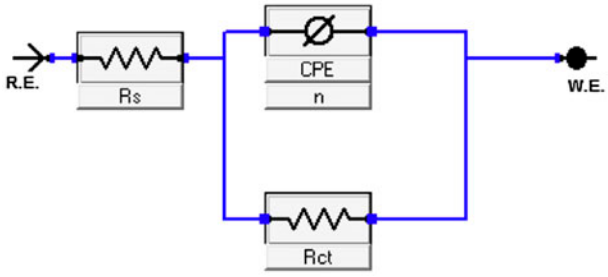

Fig. 9. The equivalent circuit model for electrochemical impedance measurements.

$$C_{dl} = (2\pi f_{max} R_{ct})^{-1} \quad (4)$$

The impedance data of the different tested materials, recorded after 30 min of the electrode immersion in different seawater samples, are presented in Figs. 10(a–d) and 11(a–c). In the natural seawater sample, Nyquist's plots for Cu displayed incomplete semicircles, denoting metal with protective oxide film [53]. While in case of Ni and Ni-Cu, it showed complete semicircle which may be attributed to the formation of an interfacial oxide layer [54].

All the investigated materials showed only one depressed semicircle in raw seawater sample and less depressed semicircles in desalinated seawater samples which can be attributed to the lack of uniformity of the current distribution. This behavior can be also related to the presence of a less uniform oxide film in the case of the natural seawater sample, which somehow induces differences in the local impedance and a time constants distribution along the electrode surface. Decreasing the seawater salinity led to increasing the diameter of the semicircle meaning that the resistance of all the tested materials against general corrosion increases with decreasing seawater salinity. The semicircles at high frequencies in Fig. 11(a–c) are generally associated with the relaxation of electrical double-layer capacitors, and the diameters of the high-frequency semicircles can be considered as the charge transfer resistance [55].

It was possible for all the investigated metals/alloy to represent the oxide charging/discharging process as a pure capacitance. However, the double-layer formation at the electrolyte-solution interface showed a time constants distribution and had to be represented by a constant phase element (CPE) [56]. This distribution is more dispersed for Cu, which has an average value 0. 57 of n_{dl}, and less dispersed for Ni-Cu and Ni with average values 0.75 and 0.84 of n_{dl}, respectively, in all tested seawater samples.

From Table 6, the charge transfer resistance (R_{ct}) values of the tested solutions increased with decreasing water salinity. Large R_{ct} values are generally associated with a slower corroding system as the R_{ct} value is a measure of electron transfer across the surface and is inversely proportional to corrosion rate [57]. However, the R_{ct} values followed the order: Ni > 70/30 Ni-Cu > Cu, it can be concluded that Ni has the highest R_{ct} value, with at least one order of magnitude greater than any other metals, whereas Cu has the lowest R_{ct} value and hence a higher corrosion rate. Therefore, corrosion rate results obtained from both potentiodynamic polarization and EIS methods confirm that Ni was the most suitable material to be used in seawater sample.

The corrosion resistance of the 70Ni-30Cu alloy is attributed to a spontaneously formed protective layer consisting mainly of a thin, inner barrier Cu_2O layer, which is in contact with the electrolyte through a thick porous outer layer of Cu(II) hydroxide/oxide [58,59]. Also, the high corrosion resistance of 70Ni-30Cu alloy compared to Cu is related to the improved electronic structure due to incorporation of nickel ions into the crystal lattice of the Cu_2O inner layer [58]. Hence, the nickel oxide dominates and the presence of Cu(II) ions does not affect their ionic or electronic property which explains the behavior of 70Ni-30Cu alloy. For this alloy, the resistance of the passive film increases,

Table 6
Electrochemical parameters derived from EIS for the studied materials in different seawater environment

Parameters	S_1			S_2			S_3			S_4		
	Cu	70/30 Ni-Cu	Ni	Cu	70/30 Ni-Cu	Ni	Cu	70/30 Ni-Cu	Ni	Cu	70/30 Ni-Cu	Ni
R_s, ohm/cm^{-2}	11.88	6.55	17	8.61	8.02	10.76	35.19	11.29	31.6	155.2	109.8	219.1
n	0.6	0.76	0.89	0.57	0.72	0.84	0.59	0.78	0.84	0.52	0.75	0.79
C_{dl}, μF/cm^{-2}	836.7	212.6	45.54	775.5	420.7	41.81	72.85	728.5	16	146.6	103.5	9.5
R_{ct}, kohm/cm^{-2}	0.24	1.513	6.775	1.297	5.329	48.92	3.888	8.732	198.8	6.897	13.77	335.6

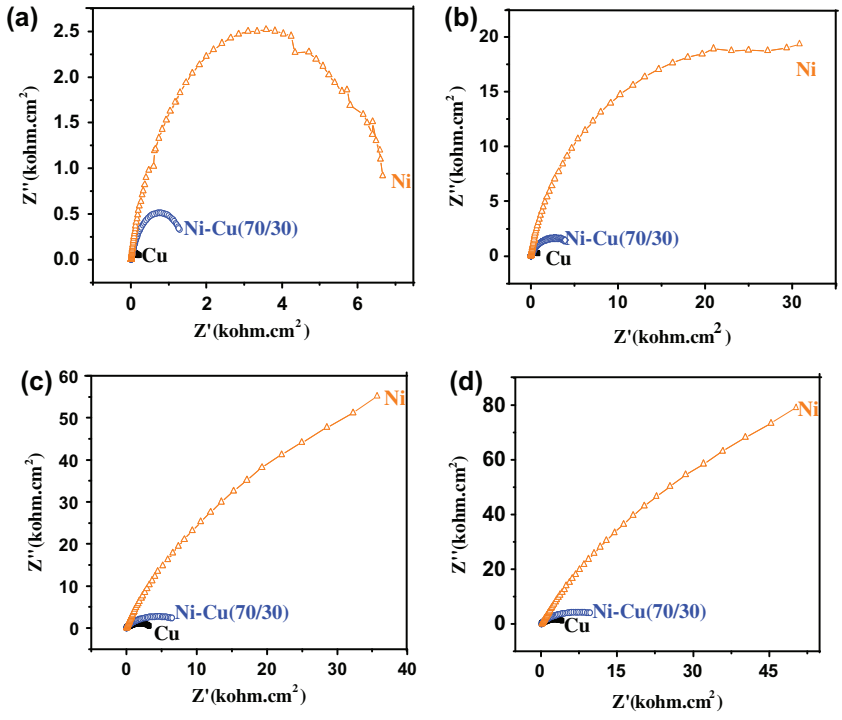

Fig. 10. Nyquist plots of the studied materials in the natural seawater sample: (a) S_1 and different desalinated seawater samples (b) S_2, (c) S_3, and (d) S_4.

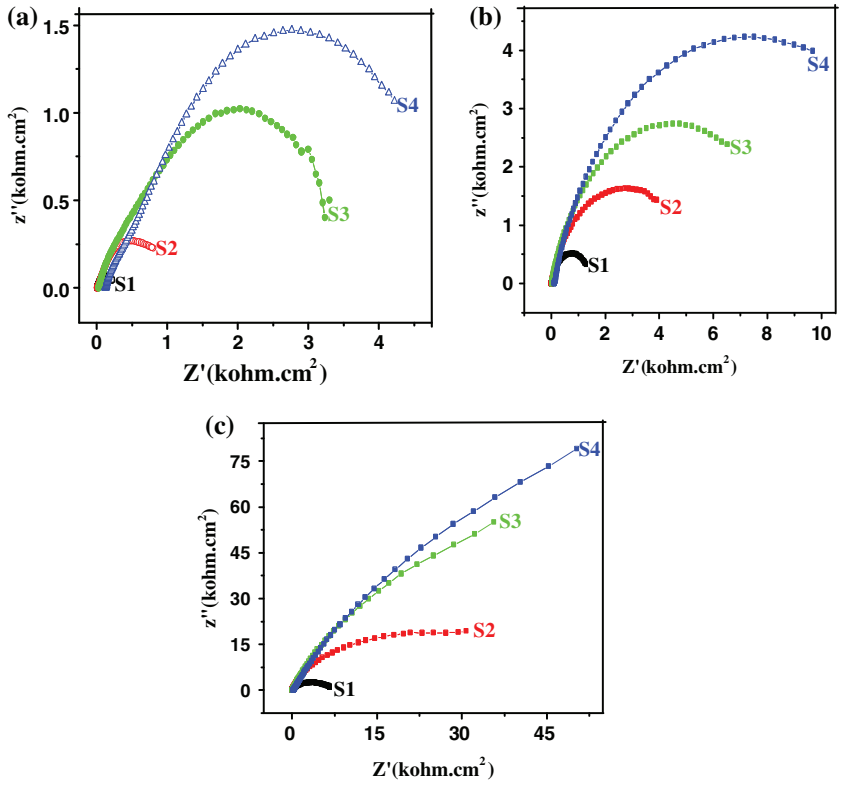

Fig. 11. Nyquist plots of the studied materials in different seawater samples: (a) Cu, (b) 70/30 Ni-Cu, and (c) Ni.

whereas its thickness decreases due to the formation of NiO.

3.5. Morphological and surface characterization

In order to study the surface morphology and to identify the composition of the corrosion products formed on the tested materials after immersion in the corrosive media, the SEM/EDX investigations were carried out.

3.5.1. SEM Characterization

Fig. 12 depicted the SEM micrographs for copper, nickel, and nickel–copper alloy after immersion for 42 d in the natural seawater (a) and desalinated seawater sample S_4 (b). SEM micrograph of copper specimens exposed to the natural seawater showed a number of pits observed on the Cu surface. The presence of chloride ions and dissolved oxygen contributed to the oxidation of the metal. It can be noticed that the copper surface is covered by aggregates of small cubic crystals $CuCl_{ads}$ and probably Cu_2O. Less damage of the surface can be noticed in the SEM image of copper immersed in desalinated samples which confirmed the decrease in corrosion rate.

Upon examination of SEM images of both nickel and Ni-Cu alloy immersed in natural seawater, the main features observed were black and white areas. The dark areas correspond to the main elements of constituents of nickel and Ni-Cu alloy, while the white areas are corresponding to sodium chloride salt presented in this area. The micrographs of nickel and

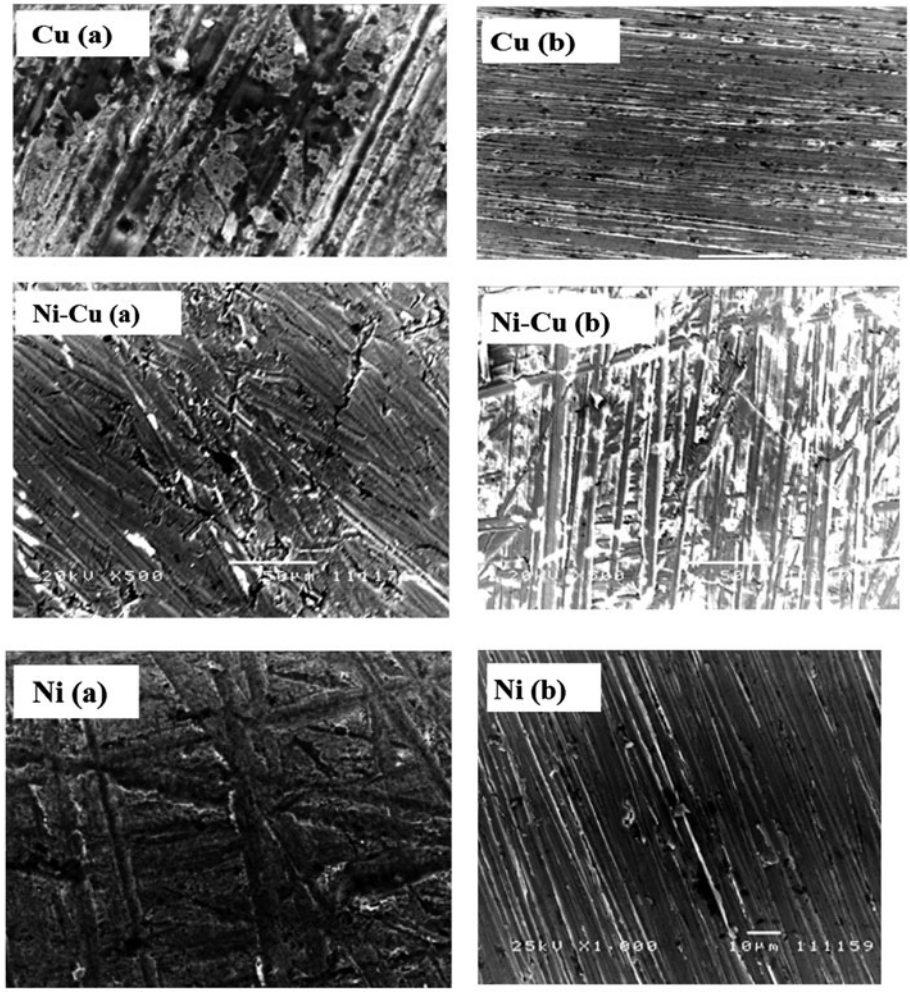

Fig. 12. Surface morphologies of the experimental materials after 42 d of immersion in: (a) natural seawater sample S_1 and (b) desalinated seawater sample, S_4.

Ni-Cu alloy immersed in the desalinated sample (S_4) indicated the decrease in the number of pits and relatively smooth surface was observed.

3.5.2. EDX analysis

The EDX technique was used to identify the elemental composition of the film formed on each investigated material. The corresponding EDX spectra for the tested materials after immersion for 42 d in the natural seawater S_1 (a) and desalinated seawater sample S_4 (b) is shown in Fig. 13. The EDX spectra of copper coupon immersed in natural seawater showed a high content of O and Cl as indicated from their high signals compared to their suppressed signals shown in the EDX profile of copper immersed in the desalinated sample (S_4). This means that in case of natural seawater media, the surface is fully covered with corrosion

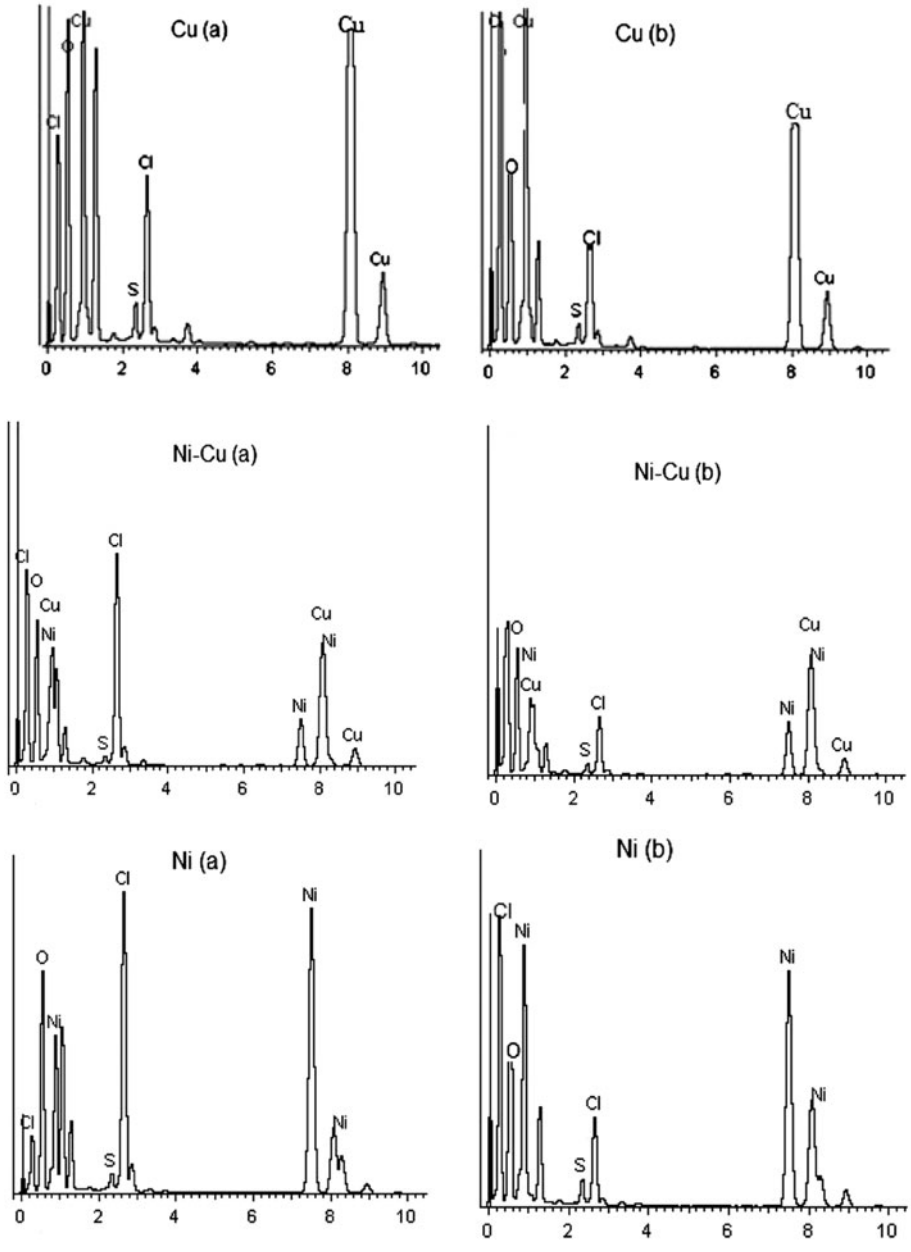

Fig. 13. EDX spectra for the studied materials after immersion for 42 d in: (a) natural seawater sample S_1 and (b) desalinated seawater sample, S_4.

products represented as thick oxide film and chloride and/or oxy-chloride compounds, while the corrosion rate decreased in desalinated sample.

EDX investigation of Ni and 70/30 Ni-Cu alloy after immersion in natural seawater (S_1) and desalinated sample (S_4) showed that both surfaces developed a mixture of most probably oxides and chlorides as indicated from O and Cl signals in EDX spectra. The low contents of Ni and Cu and the high percentages of C and O in case of Ni-Cu alloy, suggested that the alloy surface was covered with corrosion products which consist of complexes and oxides. The presence of chloride and sulfur besides oxygen also suggested that the surface had some scales which might be deposited from the seawater. Thereafter, it is clear that upon treatment of natural seawater via RO unit (S_4 sample), the content of O and Cl decreases indicating the decrease in the corrosion rate.

4. Conclusions

A natural seawater sample was treated in a semi-pilot seawater reverse osmosis (SWRO) desalination unit which was assembled in EPRI and used for producing a different seawater salinities (925, 4,845 and 18,975 mg/l TDS) to enhance the seawater properties. These different salinities were produced by mixing technique. The pretreatment processes of the natural seawater using *Amphistegina* tests demonstrated a good performance in removing particulates from the feedwater and producing permeate of acceptable quality for feeding RO membrane at temperature 40˚C and flow rate 20 l/min. The PAC appeared to be the most promising coagulant to assist the performance of the media filtration and the filtrate quality parameters, the *Amphistegina* and activated carbon filters are excellent filters for removing of TOC and iron from natural seawater. At a concentration of 1.5 mg Al/l, the SWRO desalination unit produced a good filtrate of SDI (less than 3), turbidity (less than 0.2 NTU), higher TOC% reduction (more than 97%), and the iron reduced to 0.05 mg/l.

The corrosion tests for all investigated materials, in the seawater samples with different salinities, demonstrated that the corrosion resistance of Cu, Ni, and Ni-Cu alloy is better in desalinated seawater samples than in natural seawater. These results may be attributed to the different nature of corrosion layer adherent to the tested materials. Thereafter, SEM/EDX studies indicated that pitting corrosion occurs faster for all materials in raw seawater sample and the surface develops a mixture of oxides, chlorides, and/or oxy-chloride complexes.

Acknowledgments

The authors express their thanks and appreciation to Dr Walid Makled, Exploration Department, Egyptian Petroleum Research Institute for his assistance in the manuscript production.

References

[1] M.H. Li, Reducing specific energy consumption in reverse osmosis (RO) water desalination: An analysis from first principles, Desalination 276 (2011) 128–135.
[2] C. Liu, K. Rainwater, L.F. Song, Energy analysis and efficiency assessment of reverse osmosis desalination process, Desalination 276 (2011) 352–358.
[3] J. Taylor, J. Dietz, A. Randall, S. Hong, Impact of RO desalted water on distribution water qualities, Water Sci. Technol. 51 (2005) 285–291.
[4] H. Cooley, P.H. Gleick, G. Wolff, Desalination with a grain of salt: A California perspective, Oakland, Pacific Institute for Studies in Development, Environment, and Security, CA, 2006.
[5] B. Shi, J. Taylor, Iron and copper release in drinking-water distribution systems, J. Environ. Health 70 (2007) 29–36.
[6] W. Xiao, S. Hong, Z. Tang, J. Taylor, Effects of blending on total copper release in distribution systems, J. Am. Water Works Assoc. 99 (2007) 78–88.
[7] L.F. Greenlee, D.F. Lawler, B.D. Freeman, B. Marrot, P. Moulin, Reverse osmosis desalination: Water sources, technology, and today's challenges, Water Res. 43 (2009) 2317–2348.
[8] A.A. Bakr, W.A. Makled, New pretreatment media filtration for SWRO membranes of desalination plants, Desalin. Water Treat. 55 (2015) 718–730.
[9] L. Hottinger, in: B. Leadbeater, R. Riding (Eds.), Biomineralisation in lower plants and animals, Syst. Assoc. Specifications 30 (1986) 219–239.
[10] A.A. Bakr, M.M. Kamel, A. Hamdy, K. Zakaria, M.A. Abbas, Reverse osmosis pretreatment: removal of iron in groundwater desalination plant in Shupramant-Giza-A case study, Curr. World Environ. 7 (2012) 23–32.
[11] N.P. Isaias, Experience in reverse osmosis pretreatment, Desalination 139 (2001) 57–64.
[12] FILMTEC™ Membranes, FILMTEC SW30HRLE-400 Seawater Reverse Osmosis Element, Technical Bulletin Form No. 609-00425-1107, Filmtec Membranes are Manufactured by Dow Chemical Company. Available from: <http://www.dowwatersolutions.com>.
[13] M. Schumacher, Seawater Corrosion Handbook, Park Ridge, New Jersey, 1979.
[14] D. Aylor, Seawater in: R. Baboian (Ed.), Corrosion Tests and Standards: Application and Interpretation, MNL 20, ASTM International, Pennsylvania, 1995, pp. 307–315.
[15] K.S.E. Al-Malahy, T. Hodgkiess, Comparative studies of the seawater corrosion behaviour of a range of materials, Desalination 158 (2003) 35–42.
[16] X. Liao, F. Cao, L. Zheng, Corrosion behaviour of copper under chloride-containing thin electrolyte layer, Corros. Sci. 53 (2011) 3289–3298.

[17] J. Zhang, G. Qiao, Theoretical evaluation of corrosion inhibition performance of imidazoline compounds with different hydrophilic groups, Corros. Sci. 53 (2011) 147–152.
[18] L. Feng, H. Yang, F. Wang, Experimental and theoretical studies for corrosion inhibition of carbon steel by imidazoline derivative in 5% NaCl saturated $Ca(OH)_2$ solution, Electrochim. Acta 58 (2011) 427–436.
[19] K.F. Khaled, Corrosion control of copper in nitric acid solutions using some amino acids—A combined experimental and theoretical study, Corros. Sci. 52 (2010) 3225–3234.
[20] W.A. Badawy, K.M. Ismail, A.M. Fathi, Corrosion control of Cu–Ni alloys in neutral chloride solutions by amino acids, Electrochim. Acta 51 (2006) 4182–4189.
[21] M.T. Pham, M.F. Maitz, E. Richter, H. Reuther, F. Prokert, A. Mücklich, Electrochemical behaviour of nickel surface-alloyed with copper and titanium, J. Electroanal. Chem. 572 (2004) 185–193.
[22] A. Hamdy, K. Mohammed, M.A. Abbas, A.A. M. Aly, Comparative surface study of corrosion behavior of carbon steel with nickel, copper and 70/30 Ni-Cu alloy in seawater-Part 1, Orient. J. Chem. 28 (2012) 1179–1188.
[23] Clack Corporation, Anthracite Data Sheet Form No. 2354, Replaces Form 1785, Part No. A 8029, 3 (2001) (Certified to ANSI/NSF Standard 61, Anthracite Filter Media is Manufactured by F.B. Leopold Co., Inc.).
[24] Clack Corporation, Activated Carbon Data Sheet Form No. 2348, Replaces Form 1795 & 1564, Part No. A8009-12, 3 (2011) (Certified to ANSI/NSF Standard 61, Activated Carbon is Manufactured by Calgon Carbon Corp.).
[25] D. Harvey, Modern analytical chemistry, in: James M. Smith (Ed.), Basic Tools of Analytical Chemistry, Preparing Solutions by Dilution, first ed., Library of Congress Cataloging-in-Publication Data, 1956, p. 31 (Chapter 2).
[26] Standard Test Method ASTM D 1293 for pH of water, Philadelphia, vol. 11.01, 274 (1992).
[27] Standard Test Method ASTM D 1429 for Specific Gravity of Water and Brine, vol. 11.01, Philadelphia, 301 (1992).
[28] Standard Test Method ASTM D 1125 for Electrical Conductivity and Resistivity of Water, vol. 11.01, Philadelphia, 202 (1992).
[29] A.D. Eaton, L.S. Clesceri, A.E. Greenberg, Standard Methods for the Examination of Water and Waste Water, nineteenth ed., American Public Health Association, Washington, DC, 1995.
[30] Standard Test Method ASTM D 3875 for Alkalinity in Brackish Water, Seawater and Brines, vol. 11.02, Philadelphia, 437 (1992).
[31] Standard Test Method ASTM, G 31–72, American Society for Testing and Materials, Philadelphia, PA, 1990.
[32] E.E. Abd El Aal, S. Abd El Wanees, A. Farouk, S.M. Abd El Haleem, Factors affecting the corrosion behaviour of aluminium in acid solutions. II. Inorganic additives as corrosion inhibitors for Al in HCl solutions, Corros. Sci. 68 (2013) 14–24.
[33] H. Marsh, F. Rodríguez-Reinoso, Activated carbon, (2006) 1–12 (Chapter 1).
[34] R. Don, D. Malcolm, J. Brandt, K.M. Johnson, Water supply, sixth ed., Specialized and Advanced Water Treatment Processes, 2009, pp. 365–423 (Chapter 10).
[35] G. Kear, B.D. Barker, F.C. Walsh, Electrochemical corrosion of unalloyed copper in chloride media—A critical review, Corros. Sci. 46 (2004) 109–135.
[36] F. Mansfeld, G. Liu, H. Xiao, C.H. Tsai, B.J. Little, The corrosion behavior of copper alloys, stainless steels and titanium in seawater, Corros. Sci. 36 (1994) 2063–2095.
[37] S.E. Khalid, T. Hodgkiessb, Comparative studies of the seawater corrosion behaviour of a range of materials, Desalination 158 (2003) 35–42.
[38] A. Al-Odwani, J. Carew, M. Al-Tabtabaei, A. Al-Hijji, Materials performance in SWRO desalination plant at KISR research and development program, Desalination 135 (2001) 99–110.
[39] N.A. Negm, A.M. Al Sabagh, M.A. Migahed, H.M. Abdel Bary, H.M. El Din, Effectiveness of some diquaternary ammonium surfactants as corrosion inhibitors for carbon steel in 0.5M HCl solution, Corros. Sci. 52 (2010) 2122–2132.
[40] S.N. Popova, B.N. Popov, R.E. White, D. Drazic, Determination of corrosion properties of lacquered tinplate in citrate solutions by DC and AC electrochemical methods, Corrosion 46 (1990) 1007–1014.
[41] D.A. Jones, Principles and Prevention of Corrosion, second ed., Prentice-Hall, New Jersey, 1996.
[42] J. Xu, G.L. Ruan, L. Zou, C.J. Gao, Effect of chlorine and acid injection on hollow fiber RO for SWRO, Desalination 262 (2010) 115–120.
[43] R.H. Heidersbach, Marine corrosion—Specific industries and environments, corrosion, ASM metals hand book 13(13) (1986) 893–926.
[44] J. Xiong, M.Y. Tan, M. Forsyth, The corrosion behaviors of stainless steel weldments in sodium chloride solution observed using a novel electrochemical measurement approach, Desalination 327(15) (2013) 39–45.
[45] A. Al-Hashem, J. Carew, The use of electrochemical impedance spectroscopy to study the effect of chlorine and ammonia residuals on the corrosion of copper-based and nickel-based alloys in seawater, Desalination 150(3) (2002) 255–262.
[46] J. Liang, A. Deng, R. Xie, M. Gomez, J. Hu, J. Zhang, C.N. Ong, A. Adin, Impact of seawater reverse osmosis (SWRO) product remineralization on the corrosion rate of water distribution pipeline materials, Desalination 311 (2013) 54–61.
[47] J.A. Ali, J.R. Ambrose, The relationship between copper component dissolution kinetics and the corrosion behaviour of monel-400 alloy in de-aerated NaCl solutions, Corros. Sci. 33 (1992) 1147–1159.
[48] A.M. El Din, Effect of residual and minor constituents on the corrosion behaviour of some technically important alloys, Desalination 93(1–3) (1993) 487–498.
[49] N.A. Negm, N.G. Kandile, E.A. Badr, M.A. Mohammed, Gravimetric and electrochemical evaluation of environmentally friendly nonionic corrosion inhibitors for carbon steel in 1 M HCl, Corros. Sci. 65 (2012) 94–103.
[50] M. Mahdavian, M.M. Attar, Another approach in analysis of paint coatings with EIS measurement: Phase angle at high frequencies, Corros. Sci. 48 (2006) 4152–4157.

[51] J. Hitzig, J. Titz, K. Jüttner, W.J. Lorenz, E. Schmidt, Frequency response analysis of the Ag/Ag^{+} system: A partially active electrode approach, Electrochim. Acta 29 (1984) 287–296.
[52] M.A. Migahed, Electrochemical investigation of the corrosion behavior of mild steel in 2 M HCl solution in presence of 1-dodecyl-4-methoxy pyridinnium bromide, Mater. Chem. Phys. 93 (2005) 48–53.
[53] R. Cottis, S. Turgoose, Electrochemical Impedance and Noise, NACE international series 7, Houston, TX (1999).
[54] H.P. Hack, H.W. Pickering, AC impedance study of Cu and Cu-Ni alloys in aerated salt water, J. Electrochem Soc. 138 (1991) 690–695.
[55] E.M. Sherif, S.M. Park, Effects of 2-amino-5-ethylthio-1,3,4-thiadiazole on copper corrosion as a corrosion inhibitor in aerated acidic pickling solutions, Electrochim. Acta 51 (2006) 6556–6562.
[56] M.A. Hegazy, A.M. Badawi, S.S. Abd El Rehim, W.M. Kamel, Corrosion inhibition of carbon steel using novel N-(2-(2-mercaptoacetoxy)ethyl)-N,Ndimethyl dodecan-1-aminium bromide during acid pickling, Corros. Sci. 69 (2013) 110–122.
[57] A. Istiaque, P. Rajendra, M.A. Quraisi, Adsorption and inhibitive properties of some new Mannich bases of Isatin derivatives on corrosion of mild steel in acidic media, Corros. Sci. 52 (2010) 1472–1481.
[58] R.F. North, M.J. Pryor, The influence of corrosion product structure on the corrosion rate of Cu-Ni alloys, Corros. Sci. 10 (1970) 297–311.
[59] W.A. Badawy, K.M. Ismail, A.M. Fathi, Effect of Ni content on the corrosion behavior of Cu–Ni alloys in neutral chloride solutions, Electrochim. Acta 50 (2005) 3603–3608.